A multipotent cell type from the term human placenta

Sangeetha Vadakke-Madathil[1]†, Esmaa Bouhamida[1], Bingyan J Wang[1], Prabhu Mathiyalagan[2], Parichitran Ayyamperumal[2], Amir Khan[1], Micayla Oniskey[1], Carlos Santos-Gallegos[1], Michael Hadley[1], Lori Croft[1], Fumiko Dekio[3], Rachel Brody[3], Shari Gelber[4], Rhoda Sperling[5] and Hina W. Chaudhry[1]†

[1]Department of Cardiology, Icahn School of Medicine at Mount Sinai, New York, NY, USA
[2]Benthos Prime Central, Houston, TX, USA
[3]Department of Pathology, Icahn School of Medicine at Mount Sinai, New York, NY, USA
[4]Maternal-Fetal Medicine, Icahn School of Medicine at Mount Sinai, New York, NY, USA
[5]Department of Obstetrics and Gynecology, Icahn School of Medicine at Mount Sinai, New York, NY, USA

†Co-corresponding authors: hina.chaudhry@mssm.edu, sangeetha.vadakke-madathil@mssm.edu

Abstract

We report a population of multipotent cells isolated from term human placentas, for the first time, that differentiates into cardiomyocytes and vascular cells with clonal ability, migratory ability, and transcriptomic evidence of immune privilege. Caudal-type homeobox-2 (CDX2) is a conserved factor that regulates trophectoderm formation and placentation during early embryonic development but has not previously been implicated in developmentally conserved regenerative mechanisms. We earlier reported that murine Cdx2 cells restored cardiac function after intravenous delivery in male mice with experimental myocardial infarction (MI). Here we demonstrate that CDX2 cells found in human chorion are poised for cardiovascular differentiation. We isolated CDX2 cells from term placentas of 180 healthy patients and showed that they spontaneously differentiate into cardiomyocytes, functional vascular cells, and retain homing ability *in vitro* with a transcriptome that supports enhanced cardiogenesis, vasculogenesis, immune modulation, and chemotaxis gene signatures. They restore cardiac function when administered to NOD/SCID mice subjected to MI. CDX2 cells can be clonally propagated in culture with retention of cardiovascular differentiation. Our data compel further use of this ethically feasible cell source in the design of therapeutic strategies for cardiovascular disease.

One-sentence Summary:

CDX2 cells from human placenta are poised for cardiovascular differentiation and may lead to a novel therapeutic approach for human heart repair.

Introduction

The successful use of cell therapy for cardiac repair hinges on several critical attributes: cells must have the capacity for cardiomyocyte differentiation akin to embryonic stem cells (ES) and induced pluripotent cells (iPSC), they must exhibit clonality, possess an immune-modulatory capacity for allogeneic administration, and ideally the ability to home to sites of injury. Cell therapy for cardiac purposes has been demonstrated to be safe by numerous preclinical and clinical studies(*1-4*), however; there has been a glaring lack of *bona fide* cardiac differentiation amongst cell types administered in clinical trials thus far (*5-7*). Despite a multitude of clinical cell therapy trials, which largely sought to inject stem/progenitor cells or cardiomyocytes derived from such cells into the heart, true progress in actual cardiomyocyte repopulation with a significant restoration of myocardial function has remained a distinct challenge. ES and iPS cells must be differentiated to cardiomyocytes or cardiomyocyte progenitors prior to therapeutic administration in diseased hearts, whereas we have found CDX2 cells to be committed to the mesodermal fate upon isolation from term human placentas. Our findings therefore support CDX2 cells as being naturally rooted in developmental pathways supporting organogenesis and tissue healing. Regenerative biology must rely on exploring evolutionarily preserved healing mechanisms to maintain and restore homeostasis. Gestation is one such condition that requires extensive cellular crosstalk to maintain homeostasis. The human placenta is a vital organ responsible for supporting embryonic development and facilitating the exchange of nutrients and waste between the mother and fetus. The placenta and the fetal heart are thought to undergo concurrent evolution sharing major developmental pathways (*8-10*). Studies suggest that the placenta may regulate cardiac ventricular wall expansion once maternal blood flow is established (*11-13*). This implies that cells with regenerative ability within the placenta may be better poised to support cardiogenesis. Our focus turned to placental cells after clinical observations of patients with peripartum cardiomyopathy. This etiology of heart failure enjoys the highest recovery rate (~50%) amongst all forms of heart failure (*14*) and we postulated that progenitor cells from the fetus or placenta might be playing a role in this recovery.

Stem or progenitor cells from the placenta are developmentally closer to embryonic stem cells but functionally different and non-tumorigenic (*15*). Caudal type homeobox-2 (CDX2) is a conserved transcription factor that regulates trophoblast stem cell differentiation and is required for proper placental development (*16, 17*). We discovered a novel role of Cdx2 cells in murine gestation as a preclinical model of MI in pregnant mice elicited the specific migration of fetal placental cells into the injured maternal heart to form cardiovascular cells (*18*). We later demonstrated that isolated murine placental Cdx2 lineage cells formed spontaneously beating cardiovascular cells *in vitro* and contributed to cardiac repair *in vivo* after intravenous infusion even in male mice subjected to MI (*19*).

In this study, we utilized 180 human term placentas from healthy patients and isolated CDX2-expressing cells from the chorionic regions. For research purposes, we utilized a human CDX2 promoter-driven lentivirus-based mCherry fluorescence reporter. Transcriptomic analyses comparing human embryonic cells, term placental CDX2 cells, and term placental non-CDX2 cells were performed to gain deeper insights into the functional differences between these cell types. We further investigated the stem/progenitor function, cellular heterogeneity at the single cell level,

75 and cardiovascular commitment *in vitro* and *in vivo* to ascertain their potential as a novel therapeutic for cardiovascular disease.

Results

Cells expressing CDX2 are clonal and are enriched within the chorionic region of the human placenta with a cardiovascular committed gene signature

80 The homeodomain protein CDX2 is involved in embryonic development and placentation. To detect if CDX2 is present in human placentas, we carried out a multi-parametric approach. We examined the transcript expression from an earlier time point in first-trimester chorionic villus samples (CVS) and later within the chorionic cells (fetal origin) from term healthy placentas. CDX2 mRNA was detected in CVS and chorionic regions **(Fig. 1a and Fig. S1a).** Sanger 85 sequencing and analysis of the output FASTA sequences confirmed sequences specific to human CDX2 mRNA (Data S1 Supplemental document). Immunoblot analyses detected CDX2 protein in the term chorion (~40kDa) with the conventional doublet pattern representing two isoforms from alternative splicing **(Fig. 1b and Fig. S1b, c).** HeLa cells showed a lower endogenous expression of CDX2 while H9 human embryonic stem cells (H9ESC) were negative for CDX2 90 expression (**Fig. S1d**). Human adenocarcinoma cell line DLD1 served as a positive control. Immunohistochemistry revealed that CDX2 protein was enriched in the fetal chorionic region of the human placenta and not in the fetal amnion **Fig. S1e, f**). CDX2 was detected in the villous region **(Fig. 1c and Fig. S1e)**, particularly within the cytotrophoblast layer of the chorion **(Fig. S1e).** De-identified human colon tumor tissue sections served as positive control and displayed a 95 higher CDX2 expression (**Fig. S1g**). We found that most CDX2-expressing cells co-localized with the trophoblast marker Cytokeratin 7 (**Fig. 1c, d** CKT7- 95% ± 5.0) and were associated with Human Leukocyte Antigen G (HLA-G) **(Fig. 1e, f**, HLA-G- 50.5% ± 5, also refer to **Fig. S1h, i** for individual data), which is primarily expressed in extravillous trophoblast progenitors and is critical for inducing an immune-tolerant microenvironment in the placenta.

100 The initial isolation of viable cells expressing CDX2 was challenging because no surface markers had been identified for enrichment previously. In this study, we developed a huCDX2 promoter-driven lentivirus-based approach to select cells expressing CDX2 (**Fig. S2a-c** and methods). Based on the transduction efficiency and mCherry fluorescence in DLD1 cells, out of three candidates, a sequence containing 612bps of CDX2 promoter (named as promoter 1) was 105 selected (**Fig. S2d-g**) and within the multiplicities of infection (MOI) ranging from 20-100 MOI (**Fig. S2h-q**), the 50MOI range was further chosen. To validate our lentivirus system, we also used two non-CDX2 expressing cell types and transduced CDX2mCherry lentivirus alongside CMV mCherry lentivirus (a constitutively active promoter control) in the HEK293 cell line, a human embryonic kidney-derived cell line, and human H9ESCs. **Fig. S2s** and **S2t** panels show 110 CMV mCherry fluorescence showing successful transduction with a lack of CDX2mCherry fluorescence validating the specificity of the CDX2 lentiviral reporter system.

Following isolation and initial plating, chorionic cells from term placentas were transduced with the chosen lentivirus to select CDX2mCherry positive cells (simply referred to as CDX2 cells henceforth) **(Fig. 1g)** and mCherry negative cells. A representative flow cytometry-based sort 115 profile of transduced cells is shown in **Fig. 1h.** Transduced chorionic cells from various placentas revealed that the frequency of CDX2 cells ranged from 5% to 80% with a mean frequency of 31.4% ± 3.2 **(Fig. 1i)**. Immunostaining demonstrated that the majority of mCherry signals (red) co-localized with nuclear CDX2 (green, **Fig. 1j)** validating endogenous CDX2 expression. To understand whether CDX2 cells can self-renew similarly to stem/progenitor cells, we examined

120 the clonal proliferation of single isolated CDX2 cells for a period of 14 days. CDX2 cells demonstrated a robust clonal efficiency (54.1% ± 6.78) as analyzed **(Fig. 1k, l, m)**. Interestingly, mCherry negative chorionic cells also showed the ability of clonal proliferation (44% ± 11.45). This is not surprising considering our previous report Kara et al., 2012 where we found a variety of progenitor cells other than Cdx2 cells homing to injured murine hearts. The mCherry negative
125 cells, as we noted from our transcriptomic analyses, expressed significantly higher levels of pan leukocyte marker PTPRC (CD45), myeloid progenitor marker CD33 and higher expression of CD1b suggesting more of a blood or hematopoietic lineage population **(Fig. S2r).** In addition, the mCherry negative population likely also included some CDX2 cells as the efficiency of lentivirus transduction is not 100% as clearly reflected in the positive control DLD1 cell line **(Fig.**
130 **S2u).** Response to chemotactic signaling is another key feature of stem/progenitor cells. We examined CDX2 cells for their ability to migrate to chemokine stromal-derived factor 1 α (SDF1) using a transwell migration assay. Before assessing chemotaxis, we preconditioned one group of CDX2 cells with 1μM of AMD3100, an antagonist of SDF1 receptor CXCR4. Under normal conditions, CDX2 cells exhibited a significantly higher percentage of cells migrating (22.4 ±
135 2.68%) to chemokine SDF1 compared to mCherry negative cells (12.62% ± 2.11, **Fig. 1n**). Despite the presence of SDF1 in the lower well, blocking of CXCR4 using AMD3100 significantly reduced the ability of these cells to migrate. Overall, the chemotaxis response of CDX2 cells was significantly higher than that of mCherry negative cells, and our data show that this ability may be partly mediated via a functional SDF1-CXCR4 axis.

140 CDX2 is involved in trophectoderm development, leading to trophoblast-mediated placentation, whereas embryonic stem cells are derived from the inner cell mass that significantly downregulates CDX2 expression as we see from **Fig. 1o and Fig. S1d**. To understand the developmental gene signatures, we compared CDX2 cells with H9 human embryonic cells (hESCs) and mCherry negative placenta cells in a bulk RNA sequencing analysis (Data S2 and S3
145 documents). Differential expression analysis revealed that approximately 1,065 genes were upregulated, along with 154 genes downregulated, in CDX2 cells compared with hESCs. Meanwhile, 46 genes were found to be upregulated (529 genes showing downregulation) in CDX2 cells compared to mCherry negative cells (**Table S1**).

The top 30 differentially expressed genes (DEGs) across individual samples in a biclustering
150 heatmap in comparison with H9 ES are presented in **(Fig. 1o).** The functional enrichment analysis revealed that these DEGS were involved in tissue organization, differentiation, angiogenesis, cell survival, and cardiac development. The highlighted genes **(Fig. 1o)** upregulated in CDX2 cells (and seen downregulated in hESCs involved *TBX3* and *NR2F2*, which are specifically involved in mesoderm commitment and early heart development. The downregulated genes in CDX2 cells
155 included pluripotency markers *POU5F1, FOXD3AS1, CLAUDN6, PHC1*, (*20-23*) and others (**Fig. 1o).** This lowered concerns of tumorigenicity unlike hESCs or iPSC cells (*24*). Gene ontology analyses also corresponded to functions related to immune modulation, and angiogenesis (**Fig. S3a, b**). Interestingly, migration and chemotaxis are the other key features upregulated in CDX2 cells, versus H9 ES cells, which we have functionally demonstrated above. Examining the
160 transcriptome of mCherry negative cells further, we noted an upregulated expression of genes involved in immune activation and inflammatory responses. Genes such as *RAB44*, a member of the Ras family of oncogenes, are involved in immune cell activation. Other immune activation response genes, including *EPX, CD80* (a potent immune cell marker in T and B cell activation),

and acute phase genes *ORM1, HP*, and *APOA2* (involved in HDL metabolism and atherosclerotic burden) were upregulated in mCherry negative cells **(Fig. 1p).**

Vasculogenesis-related genes were differentially expressed in CDX2 cells versus mCherry negative cells including *PECAM1* (CD31). VE-cadherin *(CDH5),* von Willebrand Factor *(vWF),* and *ACTA2* (**Fig. 1q**), which specify the angiogenic/vascular program. Pathways and genes involved in endothelial-to-mesenchymal (EndMT) transition like *SNAI2, KLF4, YAP1, VCAN* (Versican), *EGFR, CD44, TGFB2,* and *BMP4* that are implicated in valvular development were found to be significantly upregulated in CDX2 cells when compared with mCherry negative cells (**Fig. S3c, d**). A remarkable cluster of key genes implicated in mesodermal and cardiac commitment (*HAND2, DKK1, STC2, FHL1, ITGA, MYOCD, EDN1,* and *TGFB2*) was preferentially upregulated in CDX2 cells **(Fig. 1r).** These gene signatures are implicated in cardiac differentiation and cardiac tissue growth in the fetal and adult heart. CDX2 cells also significantly upregulated mesodermal, cardiac, and sarcomere organization genes, including *FHL1, STC2, DKK1, TGFB2,* and *EDN1* **(Fig. 1r)** in comparison to mCherry negative cells. These data suggest that, in contrast to undifferentiated ES cells, chorionic CDX2 cells are farther along the mesodermal/cardiac commitment pathway and that CDX2 cells are enriched for a committed cardiovascular gene signature. In sum, these data show that CDX2 cells from term placenta are trophoblast progenitor/stem cells with a unique cardiovascular gene signature.

CDX2 cells differentiate into endothelial cells and smooth muscle cells *in vitro* while they display neo-angiogenesis *in vivo*

We noted that CDX2 cells can develop endothelial vessel-like structures (27.3% ±5.6) and express endothelial markers *PECAM1* (CD31) and von Willebrand factor (*vWF*) when co-cultured with murine neonatal cardiomyocytes **(Fig. 2a-c and Fig. S4a)**. In addition, under feeder-free conditions, CDX2 cells uniformly expressed smooth muscle marker (SM22α, 95.5% ± 1.59) supporting a mesodermal phenotype **(Fig. 2d-e, and Fig. S4b)**. To examine functional angiogenesis, we assessed whether CDX2 cells could form an angiogenic network *in vitro*. Endothelial cells recapitulate angiogenesis by forming capillary-like structures when seeded onto basement membrane-like surfaces such as Matrigel. CDX2 cells displayed tubular extension and loop formation within 3h and formed endothelial-like networks after 6h. **(Fig. 2f** and **j, movie S1,** *please watch the video on loop mode*). mCherry negative cells displayed a less organized network pattern in comparison to CDX2 cells under identical conditions **(Fig. 2g, k).** HUVEC served as positive control, showing a robust tubular network at 3h and 6h time points **(Fig. 2h** and **l, movie S2,** *please watch the video on loop mode***)**. In contrast, unfractionated chorionic cells did not show any events of tube formation **(Fig. 2i, m)**. Ac-LDL uptake serves as the readout for a functional endothelium via receptor-mediated endocytosis. Therefore, CDX2 cells were primed with endothelial media containing 10ng/mL VEGF and were subjected to Ac-LDL for 4 hours, and Ac-LDL uptake was confirmed **(Fig. 2n,** green**)**. Quantification of the meshes within the endothelial network showed a significantly higher number of mesh areas in CDX2 cells **(Fig. 2o,** *$P \leq 0.05$**)** and a higher trend in the branch length, segments, and nodes, as noted **(Fig. 2p-**s**)**. We next examined the ability of functional angiogenesis of undifferentiated CDX2 cells in an immunocompromised NOD/SCID mouse model using a matrigel plug assay **(Fig. 2t)** with HUVEC cells as a positive control. After day 14, histological analyses of the excised matrigel plugs showed neoangiogenesis from CDX2 cells and mCherry negative cells, though lesser than expected compared to the differentiated HUVEC cells **(Fig. 2u)** which form mature, stable blood vessels that are typical in organized angiogenesis. CDX2 cells formed elongated vessel-like structures into and around the matrigel. Quantifying the vessel numbers showed a significant

210 increase in the CDX2 groups in comparison with mCherry negative cells (63 ± 8.7 vs 40 ± 5.3, *P≤0.05, **Fig. 2v**), whereas vessel lumen areas did not show differences **(Fig. 2w)**. Immunostaining and quantification of human-specific CD31 showed that the CDX2 cells and mCherry negative cells that formed vessels also were positive for CD31 expression **(Fig. 2x).** In sum, these data suggest that placental CDX2 cells are more angiogenic and can differentiate into
215 endothelial and vascular lineages *in vitro* and generate neo-vessels in an *in vivo* angiogenesis assay.

CDX2 cells robustly differentiate into spontaneously beating cardiomyocytes *in vitro* and significantly improve cardiac function after myocardial infarction.

We further examined CDX2 cells' ability for cardiomyocyte differentiation using a neonatal cardiomyocyte feeder system, as described in our murine studies (*19*). CDX2 cells from term
220 healthy chorions were plated on beating neonatal murine cardiomyocyte feeders, providing a niche conducive to differentiation without additional exogenous growth factors or any inducers. We previously reported the successful use of this culture system for proof-of-concept analysis (*18, 19*). Live cell imaging demonstrated CDX2 cells forming beating organoid-like clusters as early as 4-5 days in culture **(Movie S3,** *please play the video on loop mode* and **Fig. 3a)**. Within two weeks,
225 these cell clusters adhered and spread to display an elongated phenotype while they continued to beat in culture **(Fig. 3b** and **Movie S4,** *please play the video on loop mode***)**. After 4 weeks of culture, immunostaining for human-specific sarcomeric actinin, in combination with cardiac troponin T (cTnT- detects both mouse and human myocytes), demonstrated that CDX2-derived cardiomyocytes robustly expressed cardiac sarcomeric proteins with striations **(Fig. 3c-e')**. On
230 the contrary, the mCherry negative cells displayed a much lower cardiogenic capacity when cultured in identical conditions **(**5.086% ± 1.38, **Fig. S5a, d, e).** Approximately 71.11% ± 12.15 of input CDX2 cells differentiated into cardiomyocytes **(Fig. 3f)** thus displaying a high level of cardiomyogenic capacity. Even though we have separated mouse and human cardiomyocytes using specific markers, the possibility of cell fusion with feeder cardiomyocytes was further
235 excluded by in situ hybridization using mouse fluorescent XY probes (fluorescence in situ hybridization) as shown in **Fig. 3g**). Human CDX2-derived cardiomyocytes are diploid and were detected using two different human-specific probes from Empire Genomics (XX-green-dUTP 491nm-516nm) and XX- Orange-dUTP 525nm-551nm), whereas XX aqua probes (Aqu-dUTP 418nm-467nm) identified murine feeder cells after overnight hybridization. FISH analysis clearly
240 revealed the presence of only one set of sex chromosomes in CDX2-derived cardiomyocyte cell nuclei, emphasizing that CDX2–derived CMs did not exhibit cell fusion.

To understand whether a feeder-free approach can be used to differentiate CDX2 cells, we next used a temporal modulation of Wnt signaling using a modified GiWi method involving small molecule Wnt inhibitors to induce the differentiation (*25*). H9 ES cells were used as a positive
245 control for differentiation using identical culture conditions. Based on our observations from the co-culture method above, we focused only on CDX2 positive cells. As shown in the schema **(Fig. 3h)**, CDX2 cells were included in the differentiation from day 0. On day 8, day12 and day 20 after the induction, immunostaining and flow cytometry quantification for human-specific cTnT and sarcomeric actinin were carried out to examine the percentage of differentiated cardiomyocytes in
250 each group. On day 8, day 12, and day 20, the overall frequency of cardiomyocytes from input CDX2 cells was cTnT-55.45%, 85.5% and 91.7% respectively and those for sarcomeric actinin were 69.8%, 85.4% and 95.05% respectively (**Fig. 3i-j).** Representative flow cytometry data showing the progression to cardiomyocytes are shown in **Fig. 3m-o**, exhibiting a decrease in mCherry fluorescence with an increase in cTnT+ cells. We also observed sample heterogeneity
255 with regards to the retention of mCherry fluorescence after differentiation. **Fig. 3p** represents two

independent samples showing the cTnT+ population still retaining mCherry fluorescence at day 20 suggesting the inherent biological variability amongst samples.

H9ES cells expressed cTnT-22.65%, 72.5% and 82% and actinin 11.8%, 51.6% and 78% on day 8, day 12 and day 20 respectively in identical culture conditions **(Fig. 3k-l).** Interestingly, the frequency of cTnT/ actinin expressing cells on day 8 was much higher in CDX2 cells than in H9 ES cells (cTnT-22.6% in H9 vs 55.45% in CDX2 and actinin-11.8% in H9 vs 69.8% in CDX2, *p<0.05) **(Fig. 3i-l)**. We also examined the intracellular calcium response in CDX2-derived cardiomyocytes on day 20 after Fura 2AM loading. Representative ratiometric absorbance in baseline and the spikes after the addition of agonist isoproterenol is shown in **Fig. S6a, b** indicating that CDX2 derived cardiomyocytes are functional in response to calcium flux. Overall, the induced differentiation method revealed a higher efficacy of cardiac differentiation in CDX2 cells compared with ES cells. These results demonstrate that human placental CDX2 cells are highly cardiogenic and can robustly differentiate into cardiomyocytes using two different culture conditions.

To directly examine the ability of human placental CDX2 cells to elicit functional cardiac repair, we induced MI in NOD/SCID mice (9-9.5 weeks of age, male and female, **Fig. 4a**) by ligating the left anterior descending coronary artery (LAD) as we have previously *(19)*. Immediately after MI, the animals underwent intramyocardial injection with 5 µL of CDX2 cells (~100,000 cells) at each of three equidistant sites around the peri-infarct zone (n=7). Equal numbers of mCherry negative cells were also administered identically in another cohort (n=7). Vehicle control mice (n=6) received phosphate-buffered saline (PBS). Cardiac MRI was carried out immediately on the next day as post-MI baseline and also after 1-month post–MI (Fig. 4a).

Cardiac function was analyzed by clinical cardiology specialists in cardiac imaging who were blinded to the treatment arm. MRI analyses revealed a significant increase in contractility as measured by increased left ventricular ejection fraction (LVEF) in the CDX2 cell group versus vehicle controls and mCherry negative cell groups (**Fig. 4b**). This increase in cardiac function was evident when baseline LVEF of the CDX2 group (38.8 ± 2.4%) was compared to the corresponding 1-month counterparts (47.68% ± 1.8 *P≤0.05) and also between the CDX2 group and mCherry negative groups at 1-month post cell delivery. (**Fig. 4b**; CDX2 EF: 47.68% ± 1.8 vs. vehicle (PBS) controls 25.9% ± 2.3 in 1 month (***p≤0.001) versus mCherry neg group EF: 30.4% ± 3.2 (P≤0.01, ##). Representative long-axis movies of cardiac MRI images from each group are shown in Movies S5-S12 *(please play videos in loop mode),* demonstrating a clear decrease in the ventricular wall dilation in the CDX2 cell-treated group compared to the mCherry negative and vehicle control group. Individual LVEF are shown in **Table S2** and mice survival data is shown in Fig. S12. One must note here that NOD/SCID mice do not tolerate experimental MI well compared to other strains of mice and animals we have tested (*18, 19, 26*) and thus we could not induce a large enough MI to lower the immediate post-MI EF to below ~35-40% as the mice were unable to tolerate this and would die during the procedure before any intervention could be tested. This is consistent with other reports (*27*). The degree of fibrosis post-MI was evaluated in transverse histologic sections from NOD/SCID mice at 1 month after treatment with CDX2 cells, mCherry negative cells, vehicle control and sham. At least 3 sections from each of 3 different mice per group were analyzed. Fibrosis was examined using the standard Masson Trichrome assay, and 3 separate areas of each section were assessed: infarct zone (IZ), peri-infarct zone (PZ) and remote zone (RZ) **(Fig. 4c, d, e, and f).** There was a significant reduction in fibrosis in the CDX2 cell treatment group in all areas examined compared to mCherry negative cells and vehicle control. In the infarct zone, mCherry neg cell group and vehicle control showed 60.4% ± 3.08 and 78.6% ±2.7

of fibrosis respectively compared to only 46.27% ±2.5 in CDX2 cell group,****p<0.0001. In the peri infarct zone, mCherry neg cell group and vehicle control showed 46.4% ± 3.3 and 54.04% ±3.8 of fibrosis respectively compared to 28.4% ±2.4 in CDX2 cell group, ****p<0.0001. In the remote zones, mCherry neg cell group and vehicle control showed 7.8% ± 1.3 and 8.9% 1.4 of fibrosis respectively compared to 4.6 ± 0.34 in CDX2 cell group, **p<0.01. Sham had the lowest degree of fibrosis across all areas examined (average 1.26% ± 0.24). In sections from the CDX2 cell treatment group, healthy cardiac muscle was noted along both endocardial and epicardial sides of the band of fibrosis whereas this was not noted in the mCherry negative cells group or the vehicle control group. These results support the regenerative effects of CDX2 cells in the post-MI setting.

We further examined the involvement of cellular differentiation in enhanced cardiac function. Human-specific ku80 antibody as well as mCherry was used as a marker to identify injected human cells in the murine NOD/SCID hearts. CDX2 cells engrafted in the injured myocardium (**Fig. 4g**) and differentiated into cardiomyocytes expressing cTnT (green) co expressing ku80 (red) and mCherry (pink) more so in the border zone (**Fig. 4h**) with developed sarcomeres **(Fig. S7a, b),** CDX2 derived cardiomyocytes were also present in the infarct (**Fig. 4i**) and remote zones (**Fig. 4j,** also refer to **Fig. S13** to visualize individual enlarged panels of Fig.4h-i). Fig. 4k shows post-MI hearts that received mCherry negative cells, with scant or no noticeable differentiation into new cardiomyocytes (**Fig. 4l, m**). CDX2 cells contributed to vascular differentiation and co-expressed smooth muscle actin, and endothelial marker CD31 **(Fig. 4n).** mCherry negative cells also showed differentiation into vascular cells **(Fig. 4o)** however, the cardiogenic differentiation was very limited **(Fig. 4l, m**).

Quantification of the percentage of CDX2-derived vascular cells in the injury zone, border zone, and distal zone showed a trend that more CDX2 cells in the infarct and border zone expressed CD31 and SMA compared to mCherry negative cells. However, there was no statistical difference with the mCherry negative group. CDX2 cells contributed to 46.25% ± 5.556, 51.74% ± 9.83, and 13.06 % ± 4.3 of CD31+SMA+ cells in the infarct zone, border zone, and distal zone, respectively, in the post-MI heart after 1 month of cell delivery (overall 41.32% ± 5.9, **Fig. 4p, q and Fig. S7c, d**).

mCherry negative cells expressed vascular markers with a distribution of 29.4% ± 6.9, 44.03% ± 9.81, and 9.72% ± 6.2 of CD31+SMA+ cells in the infarct zone, border zone, and distal zone, respectively, contributing to an overall 31.6% ± 5.84 of vascular cells in the injured myocardium **(Fig. 4p, q and Fig. S7c, d)**. However, there was a significant increase in the cardiogenic contribution of CDX2 cells versus mCherry negative cells in the MI heart. CDX2 cells (mCherry/ku80) co-expressed cTnT and showed a distribution of 8.83% ± 4.54, 45.83% ± 7.9, and 24.72% ± 8.5 of cTnT+ cells in the infarct zone, border zone, and distal zone, respectively. mCherry negative cells rarely formed mature cardiomyocytes in the infarcted heart. There was a significant increase in the frequency of CDX2 cTnT+ cardiomyocytes in the border and distal zone compared to the mCherry negative cell group (mCherry neg- 6.25% ± 6.25, 17.22% ± 7.5, and 2.7 % ± 2.7, **Fig. 4r, s and Fig. S7 e, f**). These data indicate that more CDX2 cells were localized to the injury and border zones to augment cardiac function, as noted on MRI. CDX2-derived cTnT cardiomyocytes displayed more mature CM morphology with sarcomeric structures **(Fig. S7 a, b).** We examined the non-injured organs from NOD/SCID mice for any presence of human cells and did not find any based on flow cytometry analyses **(Fig. S7g).** This data suggests that CDX2 cells are multipotent with cardiogenic and vasculogenic potential. In contrast, the mCherry negative cell population could be vasculogenic and has very negligible cardiac differentiation ability *in vivo*,

corroborating our observations from bulk RNAseq analysis **(Fig. 1o-r)** and cellular differentiation *in vitro*. These results demonstrate that intramyocardial delivery of human placental CDX2 cells resulted in reduced fibrosis, enhanced cardiovascular regeneration, and this was associated with significant enhancement in contractile function on MRI imaging (compared to mCherry negative cells).

Single Cell RNA sequencing reveals unique cellular subsets within CDX2 cells further supporting a role for cardiovascular commitment

While culturing CDX2 cells, we noticed the overall retention of mCherry fluorescence through passages **(Fig. 5a-c)** with a significant increase in cell yield after each passage until approximately 1 million cells were generated by passage 6 based on input cell number 50,000 from only 5 gram chorionic tissue (total weight of chorionic plate is ~150 gram). Further, in a proof-of-concept experimental run, we used the Distek BioOne (Distek Inc., NJ, USA) single-use benchtop bioreactor system (BioOne1250 2L) to carry out expansion of the placental CDX2mCherry cells on microcarriers (Corning synthamax II) for 10 days. CDX2 cells showed efficient attachment and started to proliferate within the microcarrier-based bioreactor run showing a significant increase in cell yield from 7.5×10^5/mL cells to 50 $\times 10^5$ cells/mL **(Fig. 5d)** showing ~7 fold increase. CDX2mCherry cells+ microcarriers were visualized under a fluorescent microscope and we noted a significant increase in cell attachment and aggregation onto the microcarriers **(Fig. 5e, f).** Even though this was a trial run without optimization of any conditions, these data support the expansion of CDX2 cells to clinically viable numbers.

As we wished to explore further translational potential, we examined the cellular heterogeneity and cardiovascular gene program in fresh versus expanded CDX2 cells since *ex vivo* expansion will be critical to the design of a cell therapy strategy. Therefore, we performed single-cell RNA sequencing (scRNA-seq) on freshly isolated (n=2) and expanded CDX2 (passage 3, n=3) cells using 10x Genomics **(Fig. 5g).** Unsupervised clustering analysis, using the t-SNE method, revealed an unbiased distribution of 19,594 cells from the combined fresh and expanded CDX2 samples **(Fig. 5h).** Clustering of transcriptionally related cells enabled us to classify 19 subpopulations, including distinct cell populations **(Fig. S8a-c and** Data S4 document**).** Comparative analysis of gene expression profiles allowed us to identify specific trophoblast subtypes **(Fig. 5i, j)** including extravillous trophoblasts (EVTs: expressing markers *PSG1, DIO2*) constituting approximately 57.77% of the cells, and endovascular extravillous trophoblasts that are derived from EVTs (enEVT: *PRDM6*) and fibroblast-like extravillous trophoblasts (FB-like EVT: *COL1A1, CCN2*). Additionally, we identified extravillous trophoblast progenitor-like cells (EVT-TPLC: *MKI67, TOP2A*), villous cytotrophoblasts (CTB: *KRT7, EFEMP1*) (9.63%), and syncytiotrophoblasts (STB: *PGF, CGB2*) (10.51%) within the CDX2 cells. Intermediate trophoblasts, which share fewer markers of EVT, STB, and CTB, represented 19% of the total cells, with a minority of unknown cell types comprising 3%.

No significant downregulation in CDX2 expression was observed between fresh and expanded samples, although CDX2 was predominantly expressed in the STB2 cluster **(Fig. 5k, l)**. CDX2 cells expressed several key genes associated with cardiac mesoderm development, including *HAND2, GATA4, BMP4, ROR2, SMAD4, TBX3, DKK1, MSX1, MESP1, SFRP1, NKX2-5, KDR, HEY1, IRX3,* and *TBX6*. scRN-seq also corroborated the bulk RNA seq results of the enrichment of genes involved in endothelial-to-mesenchymal (EndMT) and valvular development within CDX2 cells **(Fig. S8d, e).** Importantly, in terms of cardiac gene expression, there were no significant differences between fresh and expanded samples **(Fig. 5m)** except for *SFRP1*, which

was notably upregulated in the expanded CDX2 population **(Fig. 5n and Fig. S9a)** a known antagonist of the Wnt/β-catenin pathway (*28*) and was consistent with our bulk RNA sequencing results. We observed no significant differences in angiogenesis- and vasculogenesis-related gene expression between fresh and expanded CDX2 cells **(Fig. 5o and Fig. S8b-d).** We noted that the cardiac mesoderm genes were differentially expressed across subclusters. In particular, *NKX2-5, IRX3, MSX1*, *GATA4, BMP4, HAND2, DKK1,* and *SFRP1* were highly expressed in STB clusters, with the highest levels in the STB2 subset **(Fig. 5n)**. These genes are critical regulators of cardiogenesis, essential for the specification of cardiac mesoderm and cardiomyocyte differentiation. In contrast, EVT clusters (EVT1-EVT6, enEVT2, EVT-TPLC, and FB-EVT) showed minimal or no expression of *NKX2-5*, with enEVT1 exhibiting the lowest levels. However, some cardiac mesoderm genes, such as *HAND2, ROR2, SMAD4, TBX3, SFRP1*, and *DKK1,* were variably expressed across the EVT clusters, with minimal *DKK1* expression in EVT3, suggesting EVT3 to be more angiogenic than cardiogenic. CTB clusters expressed fewer cardiac mesoderm genes than other clusters, although they still expressed *HAND2, GATA4, BMP4, MSX1*, *SMAD4, ROR2,* and *SFRP1* **(Fig. 5n).** Key genes associated with these processes, including *PECAM1, EGFR, PTGFR, KDR, HIF1A,* and *EMP1,* were highly expressed in EVT populations, while *FGF2* was significantly elevated in the STB2 subset **(Fig. 5n)**.

Within the CDX2 cell population, we discovered STB2 as highly enriched in essential cardiac mesoderm genes with FGF2, which underscores their specificity in cardiomyocyte differentiation. STB2 also expresses a higher level of CDX2 within all subclusters and co-expresses the cardiac progenitor marker *NKX2-5*. The STB2 cluster also exhibited higher levels of *MYC* and *KLF4*, transcription factors linked to cell proliferation, reprogramming, differentiation, and cardiogenesis, making it unique. In contrast, EVT populations are more associated with angiogenesis and vasculogenesis. We noted EVT3 do not express cardiogenic induction genes NKX2-5, *IRX3*, *GATA4* AND a minimal expression of *DKK1* and *BMP4* and thus appear to be enriched in vascular commitment. Additionally, we identified a unique population of EVT-TPLC characterized by proliferative gene signatures, including *MKI67, KIF23, TOP2A, ANLN, AURKA, AURKB, TEAD4, CCNA2, CDK1,* and *PCNA* **(Fig. S10a, b)** suggesting a cluster with highly proliferative genes.

Since placental cells are immune modulatory in function, we observed immune-modulatory genes like *TGFB1, CXCL10, CCL2, IL6, IL10, TNF,* and *HLA-A, -B,* and *-C,* with higher levels of *CCL2* observed in the FB-like EVT population, highlighting potential roles in immune regulation and chemotaxis **(Fig. 5n).** There were no significant differences in the freshly isolated and expanded CDX2 cells within these genes **(Fig. 5p)**. Analyses at single cell level also revealed several surface genes, including *SERPINE1, CD9*, *AQP1*, and *HMMR*. The surface marker *AQP1*, which plays a role in ion transport and cell migration, shows elevated expression in specific STB subsets. Increased expression of HMMR is known to regulate cell motility, extracellular matrix remodeling, and cell proliferation. Notably, *HMMR* is highly expressed in the STB clusters, particularly in STB2 and the progenitor cluster EVT-TPLC suggesting potential translational significance in identification of such a unique population (**Fig. S10c).** We identified additional homing genes in addition to CXCL12 and CXCR4 in our single cell analysis (**Fig. S10d**) which may help optimize homing for different subsets of CDX2 cells in future studies.

To gain insight into the differentiation potential and lineage trajectories of CDX2 populations, we performed pseudotime trajectory analysis, which enables the reconstruction of cell-state

transitions in a temporal framework (*29*). We integrated CDX2 scRNA-seq dataset with previously published scRNA-seq datasets of induced pluripotent stem cells (iPSCs), and their differentiated derivatives-CMs and ECs (*30-32*). Pseudotime analysis reveals that CDX2 cells
440 align more closely with iPS-derived CMs and ECs, clustering near these differentiated populations suggesting a developmental trajectory where CDX2 cells may serve as precursors to cardiomyocyte and endothelial lineages **(Fig. S11a).** Subpopulations of CDX2 cells positioned at different stages of pseudotime progression, suggesting heterogeneity within the CDX population. CDX2 cells near the start of the differentiation trajectory showed closer similarity to iPSCs
445 (Orange box), while those further along were transcriptionally closer to endothelial cells at D5 (Blue box) or cardiomyocytes at D30 (Green box). Interestingly, CDX2-expressing cells exhibit minimal transcriptomic overlap with ESCs and iPSCs, suggesting that they represent a distinct cellular entity rather than a conventional pluripotent stem cell population **(Fig. S11 b** and Data S5 document**).** The top 20 genes uniquely upregulated in CDX2 cells (compared to the existing data
450 base of iPSC and ES cells) included extracellular matrix genes such as *COL6A3, COL1A1, COL3A1, PALLD, FN, CD44* and *LUM* and genes associated with cardiac homeostasis including *TGM2 (33) SPON2(34), ANXA1(35), THBS1 (36),* among others. On the other hand, genes that are known to influence pluripotency; *ZFP42, PIM2, LIN28A and USP44 (37-40)* were specifically downregulated in CDX2 cells in comparison to iPSCs and ESCs. These findings have significant
455 implications, as they enable us to envision multipotent human placenta-derived CDX2 cells as an innovative approach for cardiovascular regeneration.

Discussion

In this study, we have demonstrated that CDX2-expressing cells isolated from term human placentas possess key characteristics of stem/progenitor cells and differentiate into cardiovascular
460 lineages in addition to migrating to the chemokine SDF1α. CDX2 is essential in embryonic development and is found in the trophectoderm, which in turn regulates placentation. During embryonic development, the placenta and fetal heart progress in parallel (placenta-heart axis) with the placenta regulating fetal cardiomyocyte proliferation, signifying a key functional association between these organs (*8-13*). Our findings lend credence to such a scenario as placenta-derived
465 CDX2 cells are uniquely poised to drive cardiovascular commitment and can now be viewed as a cellular target for cardiogenesis.

Various cell sources for therapeutic approaches have been studied in cardiac regeneration for decades, and the safety of such approaches has been established in clinical trials. However, finding an ideal and readily accessible cell type that can give rise to cardiovascular cells, aside from ESCs
470 and iPSCs, has proven difficult. Prenatal placental cells, particularly placental mesenchymal stem cells (PMSCs) and amniotic epithelial cells (AECs) have anti-inflammatory, angiogenic, and paracrine mechanisms that are beneficial for cardiac regenerative approaches but have not been shown to generate *de novo* cardiomyocytes (*41-43*). On the other hand, endogenous trophoblast progenitors in the placenta have not been explored for their differentiation into other cell types. Our
475 previous studies demonstrated the potential of murine Cdx2 lineage cells in the placenta to migrate to the sites of cardiac injury and produce new cardiovascular cells, significantly improving cardiac function (*19*). In a paradigmatic shift, we have now shown that multipotent human CDX2 cells are retained in the cytotrophoblasts of the human placenta through term. Our observation of the localization of CDX2 to the cytotrophoblast region is consistent with the studies of the early-
480 gestation placenta (*43*). Cytotrophoblast cells are proliferative stem cells that migrate and invade maternal spiral arteries during placentation (*44*). Similarly, we observed that CDX2 cells from human term placentas expressed villous trophoblast markers, and exhibit clonal proliferation and

migration, supporting the stem/progenitor characteristics required for cardiac regenerative approaches.

485 CDX2 cells and mCherry negative cell populations were examined in our studies using a lentivirus-based isolation method. Even though sourced from healthy placentas, differences in proliferation among various samples existed. In this study, we have also incorporated a sizable group of healthy donors of varied races which included 180 placentas, to account for any biological diversity. This approach may facilitate a more inclusive analysis as the placenta samples are 490 representative of a broader population. The selection of cells that were CDX2mCherry positive also made it easier to study the functional competency of mCherry negative counterparts from the same anatomical region of the chorion. Even though this population also exhibited clonal proliferation, we could conclusively determine that CDX2 cells have significantly enhanced cardiovascular differentiation capability compared with mCherry negative cells. The 495 transcriptomic profile of mCherry negative cells did show a reduced degree of commitment to the mesodermal lineage compared to CDX2mCherry-positive cells and their development into cardiomyocytes was minimal **(Fig. S5a-d and Fig. 4).** This could also be attributed to the incomplete targeting of all CDX2-positive cells using the lentivirus system and thus there is also a smaller number of CDX2-positive cells included in our mCherry negative group which is a 500 limiting factor in this study. Nonetheless, in comparison with mCherry negative cells and with additional hESC stem cell controls, CDX2 cells significantly upregulated chemotaxis, migration, and cardiovascular gene signatures.

Consistent with transcript analyses, human CDX2 cells generated spontaneously beating cardiomyocyte cell clusters within 5 days followed by approximately 70% of CDX2 cells 505 differentiating into cardiomyocytes on neonatal murine cardiomyocyte feeders. We carefully excluded the possibility of fusion with feeder cells by demonstrating diploid nuclei within the human CDX2 cells using XY-chromosome FISH. Remarkably, the time frame for the emergence of beating clusters was relatively shorter in CDX2 cells compared with other inductive co-culture approaches or standard protocols using pluripotent stem cells, which demonstrate the onset of 510 beating within 8–12 days (*45-47*). It is conceivable that this is because of the enriched pre-existing cardiogenic transcriptome present in the isolated CDX2 cells. These findings suggest that CDX2 cells may be a promising population for generating cardiomyocytes in a shorter time frame, which could have significant implications for regenerative medicine. We also analyzed CDX2 cell differentiation using a feeder-free, Wnt-modulated differentiation method and observed robust 515 differentiation into cTnT+ cardiac myocytes **(Fig. 3).** We noted that cardiomyocyte differentiation of CDX2 cells occurred at a faster rate than H9ES cells (a higher frequency of cTnT/actinin expressing cells within day 8) and a relatively higher percentage of cardiomyocytes were derived from CDX2 cells by day 20. As we noted further in our transcriptomic analyses, sample heterogeneity exists and mCherry downregulation and/or retention were both observed in different 520 placental CDX2 cell populations. Most importantly, comparing the standardized differentiation protocol for ES cells *(24-26),* CDX2 cells demonstrated greater efficacy of cardiac differentiation compared with ES cells.

We investigated functional cardiac repair properties of these cells by administering them to NOD/SCID mice subjected to experimental MI. There was significant enhancement of cardiac 525 function noted by MRI assessment and greater *in vivo* cardiomyocyte differentiation in the experimental group that received CDX2 cells compared to the two separate controls we used: mCherry negative cells and vehicle controls, which exhibited worsening cardiac function at 1 month post-MI. There was also significantly less fibrosis in the experimental group as compared

to the two control groups. As the CDX2 cells were human, we used NOD/SCID mice which we noted did not tolerate large infarcts well compared to previous mouse strains and animals we have utilized (*19, 26, 48*). As such we could not induce large infarcts as in our previous studies and had to limit the injury to small-moderate sized infarcts such that average baseline EF after MI was ~35-40%. We also administered the cells via intramyocardial injection for proof-of-concept whereas in mouse-to-mouse transfer previously (*19*) we administered them intravenously as the significantly larger size of human CDX2 cells were not able to traverse the mouse tail vein. It is our hope that for further preclinical studies, human CDX2 cells can be tested via intravenous and/or intracoronary administration versus intramyocardial delivery in a large animal model where the larger sized vessels will accommodate this mode of delivery. Another limitation of these infarct studies was that the use of NOD/SCID mice precludes the ability to test the immunomodulatory functions of CDX2 cells in the setting of cardiac injury, and we hope to explore these functions in future studies.

Since the placenta becomes an increasingly vascular organ during the course of gestation, cells from the placenta can be highly angiogenic. As we noted in the data from our transcriptomic analyses, endothelial tube formation from CDX2 cells suggested a strong angiogenic commitment and Ac-LDL uptake confirmed that the CDX2-derived endothelial cells are functional. In order to understand neoangiogenesis potential in non-injury conditions, we utilized the *in vivo* matrigel plug assay which revealed significantly greater vessel density induced by CDX2 cells but no significant differences in vessel area compared to mCherry negative cells. Angiogenesis is a crucial feature in cell therapy and cardiac repair, as the engraftment of adoptively transferred cells into the surrounding microenvironment is highly dependent on establishing *de novo* vasculature. Interestingly, angiogenesis and the invasive nature of trophoblast cells are interlinked as the migration potential of trophoblast cells directs endothelialization/angiogenesis during placentation (*49, 50*). On the other hand, *SDF1*-mediated chemotaxis is further involved in stem cell-mediated homing for regeneration (*51-53*) and CDX2 cells demonstrated significantly higher *SDF1*-mediated migration compared to our two control populations.

Once we established the greater cardiovascular differentiation potential of CDX2 cells by bulk RNA sequencing compared to both ESCs and mCherry negative cells, we targeted the kinetics of proliferation and differentiation at the single-cell level of freshly isolated and expanded CDX2 cells to ensure the genetic signals for cardiac differentiation were retained in expanded CDX2 cells and to provide valuable clues to address cellular heterogeneity within the placenta samples. We identified 19 subpopulations and noted there was no downregulation of CDX2 expression after expansion. Of these 19 subpopulations, there were distinct clusters that were highly cardiogenic (STBs) and others that expressed more vasculogenic genes (EVTs). There were no significant differences between angio/vasculogenesis genes and cardiogenic genes between fresh and expanded CDX2 cells. Within CDX2 cells, we discovered STB2 to be the most highly enriched cluster in essential cardiac mesoderm genes (*NKX2-5, IRX3, MSX1*, *GATA4, BMP4, HAND2, DKK1,* and *SFRP1)* along with *FGF2. FGF2* not only influences local angiogenesis and vascular stability by promoting communication with maternal tissues but also plays a crucial role in the expansion and survival of cardiac progenitor cells during development (*54*) interacting with essential pathways like Wnt and BMP (*55*), which are critical for mesodermal differentiation into cardiac lineages. Our scRNAseq also revealed immune-modulatory genes, highlighting potential roles in immune regulation and chemotaxis with no significant differences after expansion. Remarkably, single cell analysis also revealed several cell surface markers, such as *AQP1* which plays a role in ion transport and migration with elevated expression in specific STB subsets. Comparison of our CDX2 scRNAseq dataset to known scRNAseq datasets of iPSCs and hESCs

lend further support to our findings that CDX2 cells are distinct from both iPSCs and hESCs, but they map along the known differentiation trajectory of iPSCs as these differentiate to endothelial cells and cardiomyocytes.

Our findings demonstrate the functional competency of CDX2 cells from several angles critical to the development of a novel cell therapy approach, thus laying the foundations for further clinical development. The most exciting outcome of these studies is that a new progenitor cell type has been identified from a limitless source (term placenta) that differentiates into spontaneously beating cardiomyocytes as well as functional vascular cells *in vitro* and *in vivo* with enhancement of cardiac function. The diverse cellular functions exhibited by CDX2 cells provide the underpinnings for more precision-guided clinical trials of cardiac regeneration.

620

References:

625 1. A. Trounson, C. McDonald, Stem Cell Therapies in Clinical Trials: Progress and Challenges. *Cell Stem Cell* **17**, 11-22 (2015).
2. M. Xin, E. N. Olson, R. Bassel-Duby, Mending broken hearts: cardiac development as a basis for adult heart regeneration and repair. *Nat Rev Mol Cell Biol* **14**, 529-541 (2013).
3. J. Martinez, S. Zoretic, A. Moreira, A. Moreira, Safety and efficacy of cell therapies in pediatric heart
630 disease: a systematic review and meta-analysis. *Stem Cell Res Ther* **11**, 272 (2020).
4. E. Cambria *et al.*, Translational cardiac stem cell therapy: advancing from first-generation to next-generation cell types. *NPJ Regen Med* **2**, 17 (2017).
5. N. Sultana *et al.*, Resident c-kit(+) cells in the heart are not cardiac stem cells. *Nat Commun* **6**, 8701 (2015).
6. Y. Li *et al.*, Genetic Lineage Tracing of Nonmyocyte Population by Dual Recombinases. *Circulation* **138**,
635 793-805 (2018).
7. L. He, N. B. Nguyen, R. Ardehali, B. Zhou, Heart Regeneration by Endogenous Stem Cells and Cardiomyocyte Proliferation: Controversy, Fallacy, and Progress. *Circulation* **142**, 275-291 (2020).
8. G. J. Burton, E. Jauniaux, Development of the Human Placenta and Fetal Heart: Synergic or Independent? *Front Physiol* **9**, 373 (2018).
640 9. A. Mahadevan, A. Tipler, H. Jones, Shared developmental pathways of the placenta and fetal heart. *Placenta*, (2022).
10. E. J. Ward *et al.*, Placental Inflammation Leads to Abnormal Embryonic Heart Development. *Circulation*, (2022).
11. H. Shen *et al.*, Extracardiac control of embryonic cardiomyocyte proliferation and ventricular wall
645 expansion. *Cardiovasc Res* **105**, 271-278 (2015).
12. N. Witman *et al.*, Placental growth factor exerts a dual function for cardiomyogenesis and vasculogenesis during heart development. *Nat Commun* **14**, 5435 (2023).
13. R. L. Wilson *et al.*, Analysis of commonly expressed genes between first trimester fetal heart and placenta cell types in the context of congenital heart disease. *Sci Rep* **12**, 10756 (2022).
650 14. G. M. Felker *et al.*, Underlying causes and long-term survival in patients with initially unexplained cardiomyopathy. *N Engl J Med* **342**, 1077-1084 (2000).
15. E. Antoniadou, A. L. David, Placental stem cells. *Best Pract Res Clin Obstet Gynaecol* **31**, 13-29 (2016).
16. E. Maltepe, A. I. Bakardjiev, S. J. Fisher, The placenta: transcriptional, epigenetic, and physiological integration during development. *J Clin Invest* **120**, 1016-1025 (2010).
655 17. H. Niwa *et al.*, Interaction between Oct3/4 and Cdx2 determines trophectoderm differentiation. *Cell* **123**, 917-929 (2005).
18. R. J. Kara *et al.*, Fetal cells traffic to injured maternal myocardium and undergo cardiac differentiation. *Circ Res* **110**, 82-93 (2012).
19. S. Vadakke-Madathil *et al.*, Multipotent fetal-derived Cdx2 cells from placenta regenerate the heart. *Proc*
660 *Natl Acad Sci U S A* **116**, 11786-11795 (2019).
20. E. Walker *et al.*, Prediction and testing of novel transcriptional networks regulating embryonic stem cell self-renewal and commitment. *Cell Stem Cell* **1**, 71-86 (2007).
21. R. Krishnakumar *et al.*, FOXD3 Regulates Pluripotent Stem Cell Potential by Simultaneously Initiating and Repressing Enhancer Activity. *Cell Stem Cell* **18**, 104-117 (2016).
665 22. L. Chen *et al.*, PHC1 maintains pluripotency by organizing genome-wide chromatin interactions of the Nanog locus. *Nat Commun* **12**, 2829 (2021).
23. K. Wojdyla *et al.*, Cell-Surface Proteomics Identifies Differences in Signaling and Adhesion Protein Expression between Naive and Primed Human Pluripotent Stem Cells. *Stem Cell Reports* **14**, 972-988 (2020).
670 24. U. Ben-David, N. Benvenisty, The tumorigenicity of human embryonic and induced pluripotent stem cells. *Nat Rev Cancer* **11**, 268-277 (2011).

25. X. Lian *et al.*, Directed cardiomyocyte differentiation from human pluripotent stem cells by modulating Wnt/beta-catenin signaling under fully defined conditions. *Nat Protoc* **8**, 162-175 (2013).
26. S. D. Shapiro *et al.*, Cyclin A2 induces cardiac regeneration after myocardial infarction through cytokinesis of adult cardiomyocytes. *Sci Transl Med* **6**, 224ra227 (2014).
27. V. L. van Zuylen *et al.*, Myocardial infarction models in NOD/Scid mice for cell therapy research: permanent ischemia vs ischemia-reperfusion. *Springerplus* **4**, 336 (2015).
28. X. Ye *et al.*, Downregulation of Wnt signaling is a trigger for formation of facultative heterochromatin and onset of cell senescence in primary human cells. *Mol Cell* **27**, 183-196 (2007).
29. C. Trapnell *et al.*, The dynamics and regulators of cell fate decisions are revealed by pseudotemporal ordering of single cells. *Nat Biotechnol* **32**, 381-386 (2014).
30. C. E. Friedman *et al.*, Single-Cell Transcriptomic Analysis of Cardiac Differentiation from Human PSCs Reveals HOPX-Dependent Cardiomyocyte Maturation. *Cell Stem Cell* **23**, 586-598 e588 (2018).
31. D. T. Paik *et al.*, Large-Scale Single-Cell RNA-Seq Reveals Molecular Signatures of Heterogeneous Populations of Human Induced Pluripotent Stem Cell-Derived Endothelial Cells. *Circ Res* **123**, 443-450 (2018).
32. F. Soncin *et al.*, Derivation of functional trophoblast stem cells from primed human pluripotent stem cells. *Stem Cell Reports* **17**, 1303-1317 (2022).
33. F. Da Silva *et al.*, Retinoic acid signaling is directly activated in cardiomyocytes and protects mouse hearts from apoptosis after myocardial infarction. *Elife* **10**, (2021).
34. A. M. Shah *et al.*, Large scale plasma proteomics identifies novel proteins and protein networks associated with heart failure development. *Nat Commun* **15**, 528 (2024).
35. J. Chen *et al.*, Annexin A1 attenuates cardiac diastolic dysfunction in mice with inflammatory arthritis. *Proc Natl Acad Sci U S A* **118**, (2021).
36. S. M. Julovi *et al.*, Thrombospondin-1 Drives Cardiac Remodeling in Chronic Kidney Disease. *JACC Basic Transl Sci* **9**, 607-627 (2024).
37. W. Shi *et al.*, Regulation of the pluripotency marker Rex-1 by Nanog and Sox2. *J Biol Chem* **281**, 23319-23325 (2006).
38. Q. Luo *et al.*, Epiblast-like stem cells established by Wnt/beta-catenin signaling manifest distinct features of formative pluripotency and germline competence. *Cell Rep* **42**, 112021 (2023).
39. S. K. Kim *et al.*, SET7/9 methylation of the pluripotency factor LIN28A is a nucleolar localization mechanism that blocks let-7 biogenesis in human ESCs. *Cell Stem Cell* **15**, 735-749 (2014).
40. R. Yasui, A. Matsui, K. Sekine, S. Okamoto, H. Taniguchi, Highly Sensitive Detection of Human Pluripotent Stem Cells by Loop-Mediated Isothermal Amplification. *Stem Cell Rev Rep* **18**, 2995-3007 (2022).
41. R. Gorodetsky, W. K. Aicher, Allogenic Use of Human Placenta-Derived Stromal Cells as a Highly Active Subtype of Mesenchymal Stromal Cells for Cell-Based Therapies. *Int J Mol Sci* **22**, (2021).
42. Y. S. Song *et al.*, Transplanted Human Amniotic Epithelial Cells Secrete Paracrine Proangiogenic Cytokines in Rat Model of Myocardial Infarction. *Cell Transplant* **24**, 2055-2064 (2015).
43. F. Soncin *et al.*, Comparative analysis of mouse and human placentae across gestation reveals species-specific regulators of placental development. *Development* **145**, (2018).
44. F. Lyall, J. N. Bulmer, H. Kelly, E. Duffie, S. C. Robson, Human trophoblast invasion and spiral artery transformation: the role of nitric oxide. *Am J Pathol* **154**, 1105-1114 (1999).
45. X. Lian *et al.*, Robust cardiomyocyte differentiation from human pluripotent stem cells via temporal modulation of canonical Wnt signaling. *Proc Natl Acad Sci U S A* **109**, E1848-1857 (2012).
46. N. Balafkan *et al.*, A method for differentiating human induced pluripotent stem cells toward functional cardiomyocytes in 96-well microplates. *Sci Rep* **10**, 18498 (2020).
47. C. L. Mummery *et al.*, Differentiation of human embryonic stem cells and induced pluripotent stem cells to cardiomyocytes: a methods overview. *Circ Res* **111**, 344-358 (2012).
48. R. K. Cheng *et al.*, Cyclin A2 induces cardiac regeneration after myocardial infarction and prevents heart failure. *Circ Res* **100**, 1741-1748 (2007).
49. S. Piera-Velazquez, S. A. Jimenez, Endothelial to Mesenchymal Transition: Role in Physiology and in the Pathogenesis of Human Diseases. *Physiol Rev* **99**, 1281-1324 (2019).
50. Z. Alvandi, J. Bischoff, Endothelial-Mesenchymal Transition in Cardiovascular Disease. *Arterioscler Thromb Vasc Biol* **41**, 2357-2369 (2021).
51. T. Lapidot, O. Kollet, The essential roles of the chemokine SDF-1 and its receptor CXCR4 in human stem cell homing and repopulation of transplanted immune-deficient NOD/SCID and NOD/SCID/B2m(null) mice. *Leukemia* **16**, 1992-2003 (2002).

52. T. Lapidot, O. Kollet, The brain-bone-blood triad: traffic lights for stem-cell homing and mobilization. *Hematology Am Soc Hematol Educ Program* **2010**, 1-6 (2010).
53. T. T. Lau, D. A. Wang, Stromal cell-derived factor-1 (SDF-1): homing factor for engineered regenerative medicine. *Expert Opin Biol Ther* **11**, 189-197 (2011).
54. N. Rosenblatt-Velin, M. G. Lepore, C. Cartoni, F. Beermann, T. Pedrazzini, FGF-2 controls the differentiation of resident cardiac precursors into functional cardiomyocytes. *J Clin Invest* **115**, 1724-1733 (2005).
55. K. Sagomonyants, M. Mina, Biphasic effects of FGF2 on odontoblast differentiation involve changes in the BMP and Wnt signaling pathways. *Connect Tissue Res* **55 Suppl 1**, 53-56 (2014).

Acknowledgments

We thank Dr. Mone Zaidi for his review of our paper prior to submission. We thank Ms. Carolyn Quinn for helping with proofreading and editing the manuscript. We thank the Flow Cytometry Core Facility, Imaging Core Facility, Microscopy Core Facility, Biorepository and Pathology Core Facility, and Stem Cell Engineering Core at the Icahn School of Medicine at Mount Sinai for technical assistance. We acknowledge the support extended by Distek BioOne (Distek Inc, NJ, USA) for the bioreactor experiment. We thank Dr. Lisa Edelman (Genetics and Genomics Sciences, Mount Sinai) for kindly providing chorionic villous samples and we thank Dr. Lahouaria Hadri for providing reagents for the study.

Funding

National Institutes of Health grant NIH/NHLBI R01 HL150345 (HWC)

National Institutes of Health-Center for Translational Science Award (CTSA) 1KL2TR004421 (SVM)

New York Stem Cell Board funds IIRP Contract C32608GG (HWC)

Mount Sinai Innovation Partners i3 Genesis Award (HWC and SVM)

Author contributions

Conceptualization: HWC and SVM

Methodology: SVM, EB, BJW, MO

Investigation: HWC, SVM, FD, RB, SG, RS

Visualization: SVM, EB, BJW

Cardiac Imaging: CSG, MH, LC

Bioinformatics: EB, PM, PA, and AK

Clinical Inputs (patient enrollment/tissue collection): SVM, MO, FD, SG, RB, RS

Funding acquisition: HWC, SVM

Project administration: HWC, SVM, MO, FD, RB, SG, RS

Supervision: HWC

Writing – original draft: SVM, EB, BJW

Writing – review & editing: SVM, EB, BJW, AK, HWC

Competing interests

HWC the senior and co-corresponding author of this study is the inventor of an issued EU patent and US patent owned by Icahn School of Medicine at Mount Sinai (Methods of Cardiac Repair, No. 12847330.3) regarding the use of CDX2 cells for heart repair. She is also in the midst of launching a biotech that may benefit from the publication of the results presented regarding human CDX2 cells.

Data and materials availability

The new plasmids generated in this study will be made available upon publication. No unique reagents were generated from this study. Bulk sequencing and scRNA-Seq data will be made available in the NCBI Sequencing Read Archive (SRA). De-identified placental information along

with the patient's age and race/ethnicity data will be available upon request. All other data are available in the main text or the supplementary materials.

Supplementary Materials

Materials and Methods

Figs. S1 to S13

Tables S1 to S3

Movies S1 to S12

Data S1- Sanger sequencing, PEAKON and primer sequence data

Data S2 – Excel data DEG bulk RNAseq CDX2 versus H9 ES

Data S3 – Excel data DEG bulk RNAseq CDX2 versus mCherry neg cells

Data S4 – Excel data scRNA-seq- cluster based DEG of CDX2 cells

Data S5 – Excel data scRNA-seq of CDX2 cells, iPSC and human ES comparison

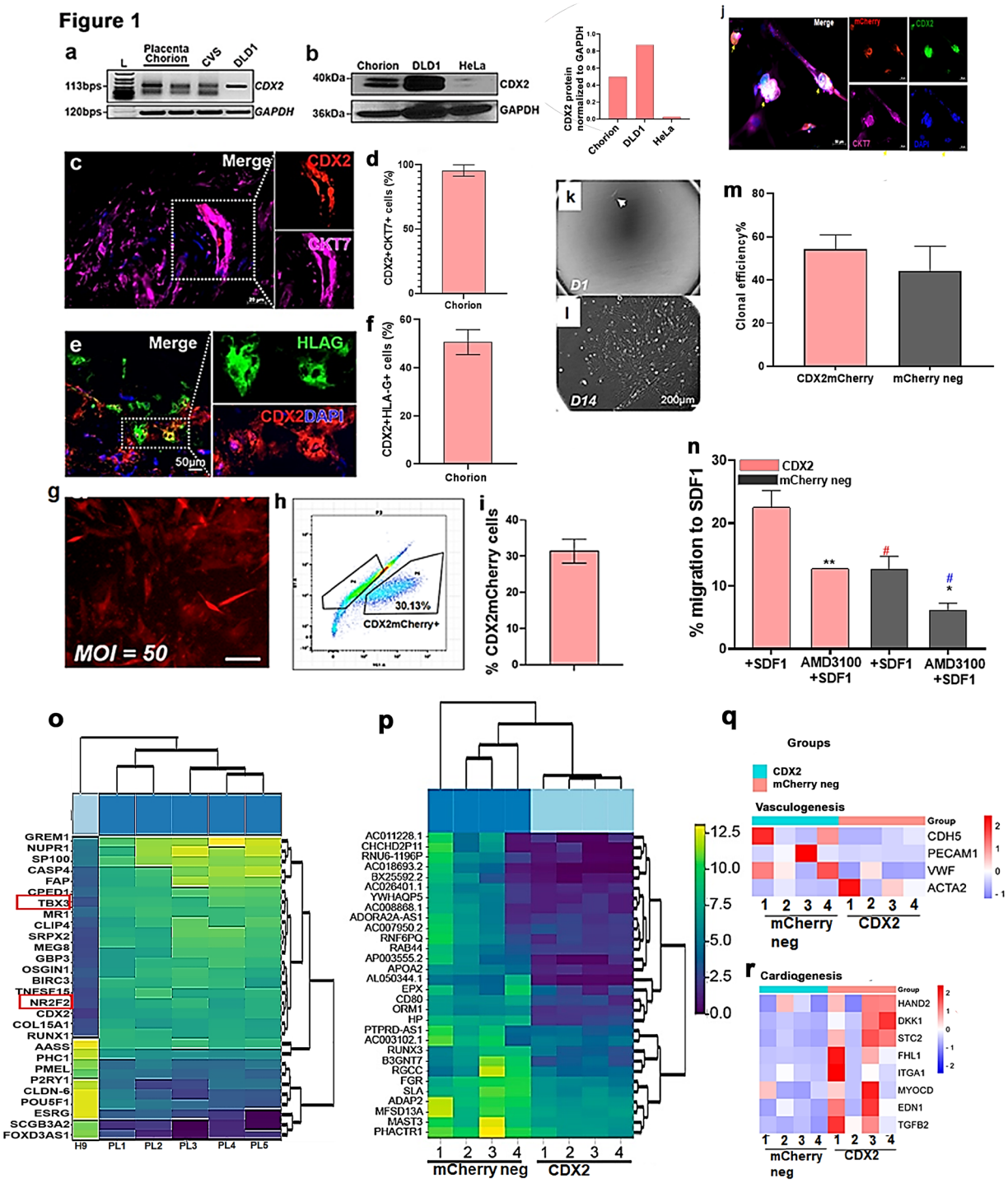
Figure 1
a
L
Placenta
Chorion
CVS
DLD1
113bps
120bps
CDX2
GAPDH
b
Chorion
DLD1
HeLa
40kDa
36kDa
CDX2
GAPDH
CDX2 protein normalized to GAPDH
Chorion
DLD1
HeLa
j
Merge
mCherry
CDX2
CKT7
DAPI
c
Merge
CDX2
CKT7
d
CDX2+CKT7+ cells (%)
Chorion
k
D1
l
D14
200µm
m
Clonal efficiency%
CDX2mCherry
mCherry neg
e
Merge
HLAG
CDX2DAPI
50µm
f
CDX2+HLA-G+ cells (%)
Chorion
g
MOI = 50
h
30.13%
CDX2mCherry+
i
% CDX2mCherry cells
n
CDX2
mCherry neg
% migration to SDF1
+SDF1
AMD3100 +SDF1
+SDF1
AMD3100 +SDF1
o
GREM1
NUPR1
SP100
CASP4
FAP
CPED1
TBX3
MR1
CLIP4
SRPX2
MEG8
GBP3
OSGIN1
BIRC3
TNFSF15
NR2F2
CDX2
COL15A1
RUNX1
AASS
PHC1
PMEL
P2RY1
CLDN-6
POU5F1
ESRG
SCGB3A2
FOXD3AS1
H9
PL1
PL2
PL3
PL4
PL5
p
AC011228.1
CHCHD2P11
RNU6-1196P
AC018693.2
BX25592.2
AC026401.1
YWHAQP5
AC008868.1
ADORA2A-AS1
AC007950.2
RNF6PQ
RAB44
AP003555.2
APOA2
AL050344.1
EPX
CD80
ORM1
HP
PTPRD-AS1
AC003102.1
RUNX3
B3GNT7
RGCC
FGR
SLA
ADAP2
MFSD13A
MAST3
PHACTR1
mCherry neg
CDX2
q
Groups
CDX2
mCherry neg
Vasculogenesis
Group
CDH5
PECAM1
VWF
ACTA2
mCherry neg
CDX2
r
Cardiogenesis
Group
HAND2
DKK1
STC2
FHL1
ITGA1
MYOCD
EDN1
TGFB2
mCherry neg
CDX2

Figure 1. CDX2 cells are clonal and are enriched in term human chorionic tissues with a transcriptome supporting cardiovascular development a) CDX2 mRNA expression in the first-trimester chorionic villous sample and term chorion from the healthy placenta. L=DNA ladder (Gene Ruler ultralow DNA ladder). Human adenocarcinoma cell line DLD1 displays a higher expression of CDX2 and hence serves as a positive control. *GAPDH* served as an internal control. **b)** Western blot analyses on term healthy chorionic samples showed CDX2 protein (40KDa) with a doublet pattern indicative of the alternate splicing. DLD1 served as a positive control, while HeLa cells as a control with low endogenous CDX2 expression. Protein expression normalized to GAPDH shown to the right **c)** Immunofluorescence detection of CDX2 in term chorion showed that CDX2 (clone CDX88-red) is mainly expressed in the villi region encompassing the cytotrophoblast cells and co-express trophoblast marker Cytokeratin 7 (pink-CKT7). **d)** Quantification of tissue sections showing the percentage of CDX2 cells co-expressing CKT7. **e)** Immunofluorescence images showing CDX2 cells co-expressing HLA-G, a crucial marker identifying extravillous trophoblast progenitors in the placenta. n=3 independent placental samples wherein 3 different ROIs from each section were screened. CDX2–Red; HLA- –Green; DAPI – Blue). **f)** Bar graph representing the percentage of CDX2 cells co-expressing HLA-G, approximately 50% (50.5±5.0%) of CDX2 cells co-expressed HLA-G. **g)** CDX2 lenti mCherry was used to transduce chorionic cells (50 MOI), and cells expressing CDX2 displayed mCherry fluorescence. **h-i)** Flow cytometry-based isolation of mCherry+ cells and quantification of CDX2mCherry positive cells from various placentas. Data are presented as mean ± SEM (n=30 independent samples). **j)** The specificity of the lentivirus-based selection of CDX2 cells was validated using CDX2mAb (CDX-88clone). Co-localization of mCherry fluorescence with CDX2 antibody (Green) and trophoblast marker Cytokeratin 7 (CKT7-pink). **k-l)** Representative phase contrast image for clonal proliferation of CDX2 cells on day 1 compared to an increase in clonal proliferation of CDX2 cells in day 14 in culture. **m)** Clonal efficiency was analyzed on day 14 and found to be 54.1 ± 6.78% in CDX2 cells versus 44 ± 11.45% in mCherry negative cells. Data are presented as mean ± SEM (n=4 independent samples). **n)** *In vitro* homing of CDX2 cells and mCherry negative cells to chemokine SDF1 is partially dependent on the CXCR4 axis. CDX2 cells show significantly higher migration in both conditions compared to mCherry negative cells. Data are presented as mean ± SEM (biological replicates comprising 3 independent samples *$p<0.05$, **$p<0.01$). **o)** Bi-clustering heatmap showing the expression profile of the top 30 differentially expressed genes in CDX2 cells (labeled 1-5) versus hESCs (H9 ES ctrl pooled extreme left) in bulk RNAseq analyses. Genes were sorted by their adjusted p-value by plotting the log2 transformed expression values. The yellow-green color code indicates the upregulated and the blue-gray color code indicates the downregulated genes across the samples. CDX2 cells showed upregulated cardiac mesoderm commitment genes *(NR2F2* and *TBX3,* highlighted in red box*)* while downregulating pluripotent markers *CLDN6*, *POU5F1,* and *ESRG.* **p)** A bi-clustering heatmap with the top 30 differentially expressed genes showing the upregulated function of inflammatory response and immune genes in mCherry negative cells (n=4 independent samples in each group).**q)** Heatmap depicting the vasculogenic genes *(PECAM1, CDH5,vWF* and *ACAT2)* in both CDX2 and negative cells. **r)** Heatmap showing cardiogenic genes *(HAND2, DKK1, STC2, FHL1, ITGA1, MYOCD EDN1,* and *TGFB2)* in both CDX2 and negative cells

Figure 2

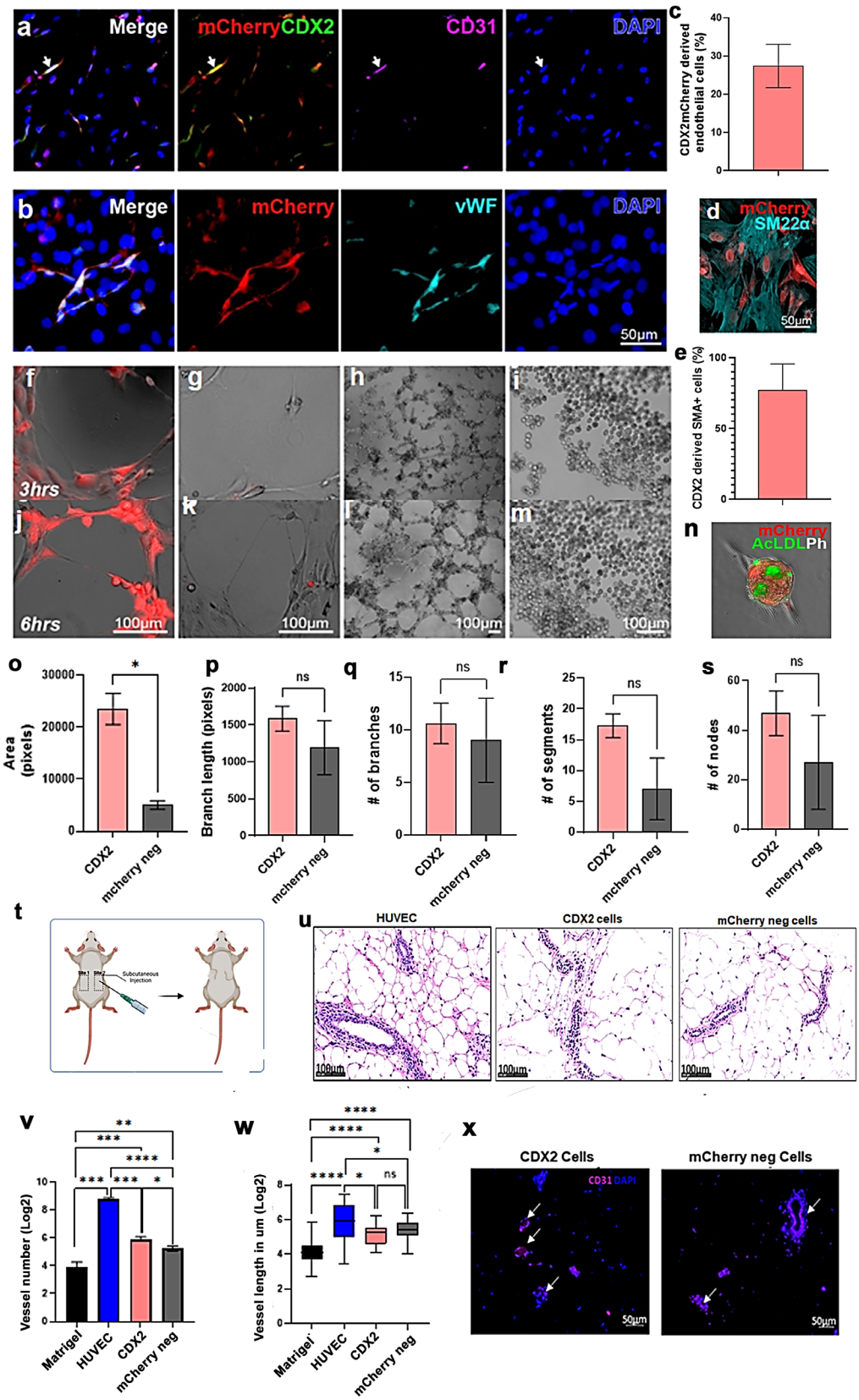
a
Merge
mCherryCDX2
CD31
DAPI
b
Merge
mCherry
vWF
DAPI
50µm
c
CDX2mCherry derived endothelial cells (%)
d
mCherry
SM22α
50µm
e
CDX2 derived SMA+ cells (%)
f
3hrs
j
6hrs
100µm
g
k
100µm
h
l
100µm
i
m
100µm
n
mCherry
AcLDLPh
o
Area (pixels)
p
Branch length (pixels)
q
# of branches
r
# of segments
s
# of nodes
ns
CDX2
mcherry neg
t
Subcutaneous Injection
u
HUVEC
CDX2 cells
mCherry neg cells
100µm
v
Vessel number (Log2)
Matrigel
HUVEC
CDX2
mCherry neg
w
Vessel length in um (Log2)
x
CDX2 Cells
mCherry neg Cells
CD31 DAPI
50µm

855

Figure 2. CDX2 cells are angiogenic and display endothelial tube formation *in vitro* and *in vivo*. **a**) Subset of CDX2 cells (red) expressed vascular lineage marker CD31 (pink) and further
860 gave rise to blood vessel-like assembly (and stained positive for endothelial marker von Willebrand Factor (vWF-green) upon co-culture with neonatal cardiomyocytes **(b, c)**. Data represented as mean±SEM of four independent samples (n=4). **d, e)** CDX2mCherry cells also expressed smooth muscle marker (SM22α) upon feeder-free culture using IMDM+10%FBS. **f)** Endothelial tube formation by CDX2mCherry cells on matrigel in 3hrs and **j)** the formation of
865 endothelial-like networks within 6hrs, also refer to movie S1. **g, k)** mCherry negative cells showing networks, albeit not as intact and optimal as their CDX2mCherry counterpart on matrigel. **h, l)** Human umbilical vein endothelial cells (HUVEC) served as a positive control, also refer to movie S2). **i, m)** Total chorionic cells from the placenta did not exhibit endothelial tube formation at both time points. **n)** Ac-LDL (Alexa-488) uptake by primed (M200 medium +LSGS+ 10ng/mL VEGF)
870 CDX2mCherry cells suggesting the formation of a functionally active endothelium. **o-s)** Quantification of the endothelial network using ImageJ software with an angiogenesis analyzer showed a higher endothelial loop-like area and branching segments compared to mCherry negative cells (n=5 independent CDX2mCherry positive and n=2 independent mCherry negative samples with biological triplicates per assay). **t**) Schematic image overview of the experimental plan of the
875 matrigel plug assay for angiogenesis assessment (n=3 per group). **u)** Representative microscopic images of hematoxylin and eosin (H&E) (20× magnification) of HUVEC, CDX2 cells, and negative cells. **v)** Bar graph showing the vessel numbers and **w)** a box and whisker plot representing the vessel areas in HUVEC cells, CDX2 cells, and negative cells., where CDX2 cells showed significant increase in vessel numbers,*$P \leq 0.05$ **x)** Representative immunofluorescence
880 images showing CD31 (purple) and DAPI (blue) staining in both CDX2 and mCherry negative cells.

885

890

895

900

Figure 3

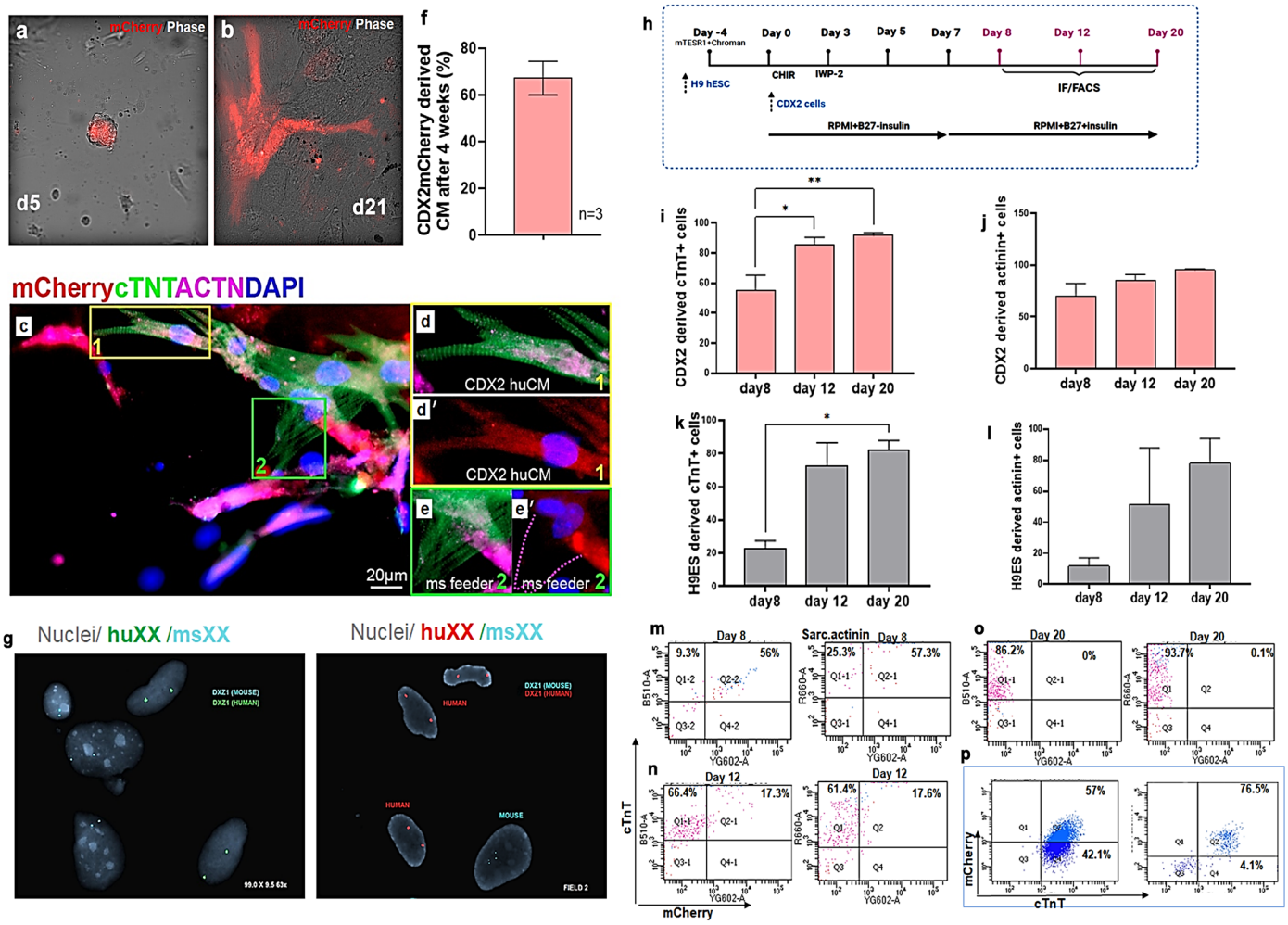

Figure 3. CDX2 cells differentiate into spontaneously beating cardiomyocytes. a) Snapshot of a beating CDX2mcherry cell cluster on day 5 on co-culture with murine neonatal cardiomyocytes feeder (non-mCherry-gray cells in the background), also see movie S3. *Please watch in loop mode.* **b)** Snapshot of beating-adhered and elongated CDX2mCherry cardiomyocytes 3 weeks in culture (movie S4, *Please watch in loop mode*). **c)** CDX2-derived cardiomyocytes (mCherry-red) stain positive for human cardiac sarcomeric actinin (pink-Alexa 647) and (cTnT-green Alexa 488). The specificity of the human actinin antibody was detected by a lack of staining on murine feeder myocytes in the background, while cTnT (green) detects both mouse and human cardiomyocytes. Yellow box 1 is further highlighted to the right. **d** and **d')** showing the striated sarcomeres visible on human CDX2 mCherry-derived cardiomyocytes (actinin pink + cTnT green+). Meanwhile, green box 2 and the expanded panels point to the endogenous murine feeder myocyte that expresses only cTnT (green). **e** and **e').** Nuclei are counterstained using DAPI (blue). **f)** Quantification

920 revealed that approximately 71.11% ± 12.15 of input CDX2 cells differentiated into cardiomyocytes. Data are represented as mean ± SEM (n=5 independent samples). **g)** Cell fusion with feeder murine cardiomyocytes were ruled out by XY chromosome FISH analyses. Human cells are diploid and were detected using two different human-specific probes from Empire Genomics (XX- green-dUTP 491nm-516nm) and XX- Orange-dUTP 525nm-551nm), whereas XX aqua probes (Aqu- dUTP 418nm-467nm)
925 identified murine feeder cells after overnight hybridization. FISH analysis clearly revealed the presence of only one set of sex chromosomes in CDX2-derived cardiomyocyte cell nuclei, emphasizing that CDX2–derived CMs did not exhibit cell fusion (n=3). **h)** Feeder-free differentiation of CDX2 cells using temporal modulation of Wnt signaling. Schema of GiWi experimental outline. H9ES cells were used as controls under identical culture conditions. CDX2 cells isolated from three different term placenta samples were included
930 on day 0 with the beginning of the Wnt activation step followed by sequential induction steps until day 20. **i-j)** Cardiac-specific markers cTnT and sarcomeric actinin were used to quantify differentiation on day 8, day 12 and day 20 showing an efficient differentiation of CDX2 cells as early as day 8 in comparison to **(k, l)** H9ES cells at the same time point. **m-o)** Representative flow cytometry profiles showing time course of differentiation of CDX2 cells into cTnT (B510A-Yaxis) and actinin (R660A-Yaxis) expressing cells
935 downregulating mCherry fluorescence from day 8- day 20 from same sample (n=4). **p)** Data from a different CDX2 cell population still retaining mCherry expression (mCherry+cTnT+) on day 20 of differentiation indicting inter variability among placental samples.

940

945

950

955

960

965

970

Figure 4

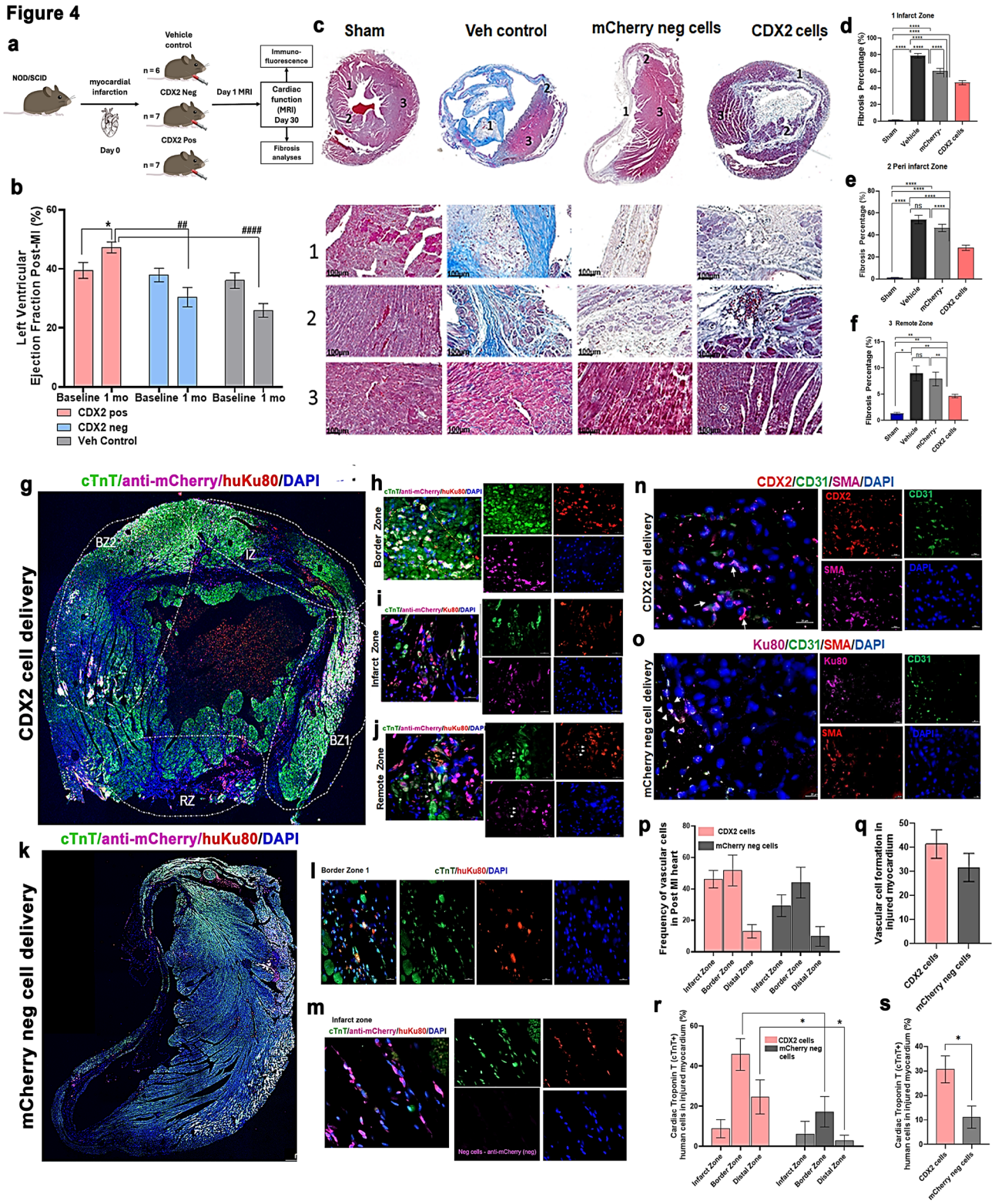
a
NOD/SCID
myocardial infarction
Day 0
Vehicle control
n = 6
CDX2 Neg
n = 7
CDX2 Pos
n = 7
Day 1 MRI
Immuno-fluorescence
Cardiac function (MRI) Day 30
Fibrosis analyses
b
Left Ventricular Ejection Fraction Post-MI (%)
Baseline 1 mo Baseline 1 mo Baseline 1 mo
CDX2 pos
CDX2 neg
Veh Control
c
Sham
Veh control
mCherry neg cells
CDX2 cells
d
1 Infarct Zone
Fibrosis Percentage (%)
e
2 Peri infarct Zone
f
3 Remote Zone
g
cTnT/anti-mCherry/huKu80/DAPI
CDX2 cell delivery
BZ2
IZ
BZ1
RZ
h
Border Zone
i
Infarct Zone
j
Remote Zone
k
cTnT/anti-mCherry/huKu80/DAPI
mCherry neg cell delivery
l
Border Zone 1
cTnT/huKu80/DAPI
m
Infarct zone
cTnT/anti-mCherry/huKu80/DAPI
Neg cells - anti-mCherry (neg)
n
CDX2/CD31/SMA/DAPI
CDX2 cell delivery
CDX2
CD31
SMA
DAPI
o
Ku80/CD31/SMA/DAPI
mCherry neg cell delivery
Ku80
CD31
SMA
DAPI
p
CDX2 cells
mCherry neg cells
Frequency of vascular cells in Post MI heart
Infarct Zone
Border Zone
Distal Zone
q
Vascular cell formation in injured myocardium
CDX2 cells
mCherry neg cells
r
Cardiac Troponin T (cTnT+) human cells in Injured myocardium (%)
s

975

Figure 4. CDX2 cell delivery significantly improved cardiac function after myocardial infarction. a) Experimental design for the myocardial infarction experiment using NOD/SCID mice. **b)** Cardiac MRI analyses showing a significant increase in left ventricular ejection fraction (EF) in CDX2 cell-injected mice versus the control animals at 1-mo time points compared with
980 the baseline MI timeline (CDX2 group, n = 7; mCherry neg group, n = 7, Vehicle control PBS n=6). Data are represented as mean ± SEM. *P≤0.05 (CDX2 baseline MI vs. 1 mo post-MI), ##P≤0.01 (CDX2 at 1 mo vs.mCherry neg at 1 mo post-MI) and ####P≤0.0001 (CDX2 1mo post-MI vs. PBS group 1 mo post-MI). **c)** Trichrome analyses to visualize MIs and to evaluate fibrosis percentage showing representative myocardium from sham (no MI), veh control (MI+PBS
985 injection), MI+CDX2 cell injection and MI+mCherry negative cell injection group (3 slides from each of 3 mice/group examined). Fibrotic areas are stained blue (collagen), and viable tissue is stained red (muscle). Images of Infarct zone (1), Peri infarct zone (2) and Remote Zone (3) are shown in the bottom panel with **d-f** presenting quantified fibrosis percentages**.** Data shows a significant reduction in fibrosis in CDX2 cell group compared to mCherry neg cell injected and
990 PBS injected mice post MI. Data are represented as mean ± SEM. (*p<0.05, **p<0.01, ***p<0.001 and ****p<0.0001). **g)** Engraftment of CDX2 cells (anti-mCherry pink, huKu80 red) in post-MI heart and differentiation into cardiomyocytes expressing cTnT in the **h)** border zone (**also refer to Fig. S7 a, b** showing sarcomere structure), **i)** infarct zone and **j)** in remote zones. **Please refer to Fig. S13** to visualize enlarged images from h-j. **k)** mCherry negative cells (Ku80-red) in the
995 injured myocardium 1 month post-MI. Limited cardiogenic contribution of mCherry negative cells in injured myocardium.-cardiomyocytes (CMs) are immunostained for (cTnT-green) in **l,m)** border zone and infarct zone. **n)** CDX2 cells and mCherry neg cells contributed to vascular differentiation *in vivo*. (Scale bar: 20 µm) Border zone shows CD31+ SMA+ cells associated with mCherry (CDX2 group-n) or Ku80 (mCherry neg group- **o)** highlighted with white
1000 arrows. **p)** Quantification of distribution of CDX2 and mCherry neg derived vascular cells in infarct, border and remote zones and **q)** total vascular cell contribution of CDX2 and mCherry neg cells. **r)** distribution of CDX2 and mcherry neg cell-derived cardiomyocytes in the infarct, border, and distal zones, demonstrating significantly higher cardiogenic potential of CDX2 cells *in vivo* *P≤0.05 and **s)** Quantification of overall cardiomyocytes and data are presented as mean
1005 ± SEM.

1010

1015

1020

1025

Figure 5

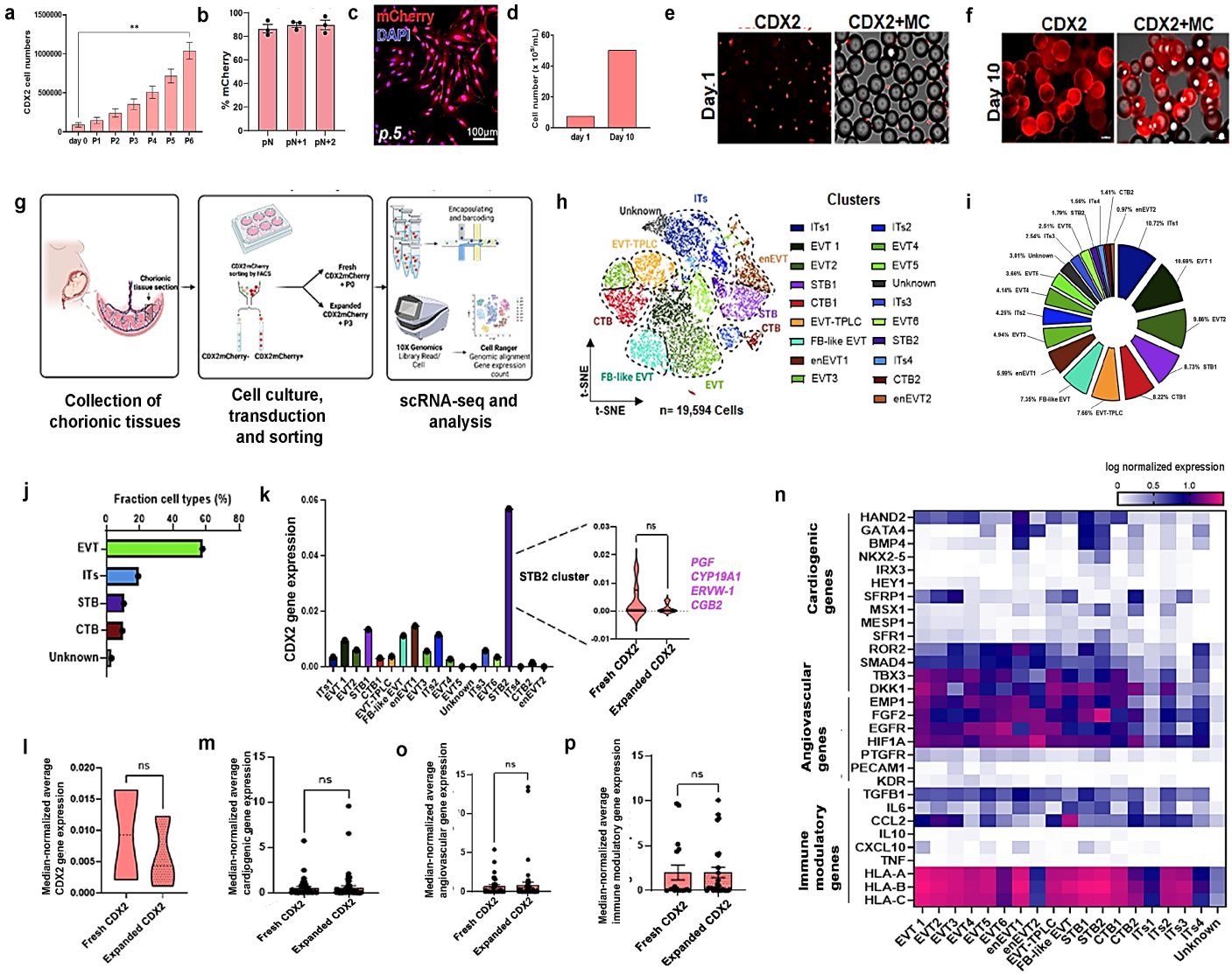

1030

Figure 5. *Ex vivo* expansion and transcriptomics analyses revealing cardiovascular commitment and unique cellular subclusters in placental CDX2 cells at single cell level. a) Quantification of mCherry cells after expansion showed a significant increase of up to 1 million cells by passage 6 compared to day 0 of isolation. Data represented as mean ± SEM (n=3, *p<0.05, **p<0.01). **b)** Retention of mCherry expression over the various passages as analyzed by flow cytometry and **c)** representative fluorescent microscopy image at p5. **d**) A representative bar graph showing the cell yield of CDX2 cells on day 1 versus day 10 of the bioreactor culture. **e)** Representative fluorescence microscopy images showing a remarkable difference in cell attachment and proliferation of CDX2 cells (mCherry) on synthemax II microcarriers at the beginning (1 day) and the **f)** end (day 10) of bioreactor based expansion. Data are representative of pooled CDX2 cells isolated and expanded from 3 different placenta samples. **g**) Schematic representation of the workflow for isolating and analyzing human placental CDX2 cells using single-cell transcriptomics. **h**) T-distributed Stochastic Neighbor Embedding (t-SNE) analysis of human placental CDX2 cells, both fresh (n=2) and expanded (n=3) and the different cluster groups. Each dot represents a single cell, with different colors indicating distinct cell types. Villous cytotrophoblasts (CTB), syncytiotrophoblasts (STB), extravillous trophoblasts (EVT), Endovascular extravillous trophoblast (enEVT), EVT-trophoblast progenitor-like cells (EVT-TPLC), Fibroblasts like trophoblasts (FB-like EVT), Intermediate trophoblasts (ITs) and Unknown cells. **i**) Pie chart showing the percentages of CDX2 subclusters. **j**) Column chart showing the fraction of indicated cell types **k)** Bar graph depicting CDX2 expression levels across different clusters in both fresh and expanded CDX2 cells, with emphasis on the STB2 cluster, which exhibits higher CDX2 expression and is present in both fresh and expanded populations **l**) Violin plot showing CDX2 gene expression in both fresh and expanded CDX2 cells. **m**) Representative graph illustrating cardiogenic gene expression levels in fresh versus expanded CDX2 cells. **n**) Heatmap displaying the expression levels of cardiogenic, angiogenic/vasculogenic, and immune-modulatory genes across various clusters of CDX2 cells**. o)** Bar graph depicting the expression levels of vasculogenic genes in fresh and expanded CDX2 cells. **p**) Bar graph showing the expression levels of immune-modulatory genes in fresh and expanded CDX2 cells.